Engineering Structures 305 (2024) 117743

Contents lists available at ScienceDirect

Engineering Structures

journal homepage: www.elsevier.com/locate/engstruct

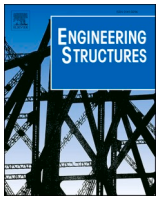

Shear strengthening of precast prestressed bridge I-girders using shape memory reinforcement

Muhammad Arslan Yaqub [a], Christoph Czaderski [b,*], Stijn Matthys [a]

[a] Magnel-Vandepitte Laboratory, Department of Structural Engineering and Building Materials, Ghent University, Ghent, Belgium
[b] Empa, Swiss Federal Laboratories for Materials Science and Technology, Dübendorf, Switzerland

ARTICLE INFO

Keywords:
Prestressed concrete (PC) I-girder
Shear strengthening
Iron-based shape memory alloy (Fe-SMA)
Active shear strengthening
Truss analogy

ABSTRACT

Existing bridge infrastructure requires careful monitoring, assessment and in some cases application of a suitable rehabilitation system to ensure proper operation through the service life of the structure. A large number of existing concrete bridge structures are composed of prestressed concrete (PC) I-girders that, either due to aging or more stringent design provisions, require rehabilitation. Research in the past has revealed challenges associated to shear strengthening of I-shaped girders with externally bonded fibre reinforced polymer (FRP). Given the concave shape of the cross section with bonded FRP, there is a tendency of severe debonding at the web-flange interface. Therefore, interest arises for more reliable solutions for shear strengthening of such an important cross section that is widely used in the concrete bridge industry. In search of an effective shear strengthening solution for PC I-girders, this study reports a detailed experimental program that uses memory steel reinforcement in the form of plain strips or ribbed rebars that are used as externally applied shear reinforcement in order to enhance the shear capacity. When fixed to the cross section, memory steel has an intrinsic property of recovering pre-induced strains during heating and subsequent cooling, as a result of which lateral prestressing is applied to the cross-section. Iron-based shape memory alloy (Fe-SMA) strips were wrapped and anchored at the top of the PC I-girder cross section, while, ribbed Fe-SMA rebars were used as near surface mounted (NSM) reinforcement. Each system was assessed in two different ways i.e. with and without heating/activation of the Fe-SMA shear reinforcement, in order to observe the difference between passive and active (prestressed) shear reinforcement. Fe-SMA shear strengthening provided an increase of 40 to 47% in the shear capacity of the studied PC bridge I-girders, whereby four full scale shear tests were executed in comparison to that of a control specimen without strengthening. The activated Fe-SMA shear strengthening configurations helped in controlling shear crack widths and showed better serviceability performance compared to the passive counterparts. Truss analogy for shear design has been applied to assess the shear contribution of Fe-SMA shear reinforcement, resulting in close estimation.

1. Introduction

Concrete bridges constitute a major part of transportation infrastructure that is a key to the socio-economic strength of a region, so it requires proper maintenance, repair or upgrading. To ensure the long run serviceability of existing concrete bridges, timely assessment and (in some cases) rehabilitation is desired. This to solve for the degradation of the bridge structure subjected to increased traffic loads, impacts from vehicles or to rationalize the effects of improper design and detailing, as well as aging. Moreover, at present, the capacity enhancement of a bridge structure can also become essential to account for the improved design provisions that are more reliable. The American Road and Transportation Builders Association reported that every 1 out of 3 bridges need repair or replacement. This corresponds to more than 43500 bridges that are rated in poor condition and the rehabilitation of these bridges will take up to 30 years or more [1]. In Europe, the scale of this problem is similar, however, aggregated data on the number of bridges requiring rehabilitation is not easily available, as every member country has its own assessment protocols and different levels of priority based on the type and use of the bridge structures. Concerning existing concrete bridges that are potentially shear deficient, a careful assessment is necessary, as the shear failure mode is undesirable. Damages due

* Corresponding author.
E-mail address: christoph.czaderski@empa.ch (C. Czaderski).

https://doi.org/10.1016/j.engstruct.2024.117743
Received 9 October 2023; Received in revised form 12 January 2024; Accepted 20 February 2024
Available online 2 March 2024

to shear in existing concrete bridges is not an apparent physical problem but it becomes a great concern if such structures are evaluated using the latest design guidelines or if the structure demands for another strengthening intervention, for example, flexure strengthening. Pre-stressed I-shaped girders are a common concrete bridge component, which is difficult to strengthen in shear subject to its concave shape, associated to the I-shaped cross-section. Attempts were made in the past to shear strengthen I-girders using externally bonded carbon fiber reinforced polymers (CFRP), illustrating a consistent problem of early debonding around the web-flange corners of the I-girder, resulting in no or limited increase in the shear strength, despite using various kind of anchorages [2–6]. The effectiveness of CFRP as externally bonded shear reinforcement in case of rectangular beams [7] and T-beams [8,9] is well acknowledged, however, the concave shape of the I-girder makes it difficult to strengthen in shear using externally bonded CFRP. This is due to straightening of the fibers and subsequent early debonding around the web-flange corner resulting in pronounced underutilization of the CFRP when applied directly to the I-shaped concrete surface. An alternative technique (recently investigated by the authors) uses concrete in-fill blocks to transform the I-shape into a rectangular shape, with CFRP strips bonded over the in-fill blocks and anchored in the compression flange [10]. This technique illustrated great potential by resisting, for the tested configuration, an additional shear load up to 40%. A similar shear strengthening approach for I-girders has also been applied in another large scale study [11], and was combined with flexural strengthening by means of prestressed CFRP. For a further state-of-the-art overview on shear strengthening of I-girders using CFRP, reference is made to the comprehensive study [12].

Passive shear strengthening systems often require relatively large deformations (shear crack opening) before they actually start resisting the shear loads. Instead, active (prestressed) shear strengthening provides confinement just after the application of the prestress. A few significant advantages of prestressed shear strengthening include the active control on existing and expected shear cracks, reduction of the stress level in the internal shear reinforcement and active contribution against additional loads just after the application of the strengthening system [13]. Bonded CFRP represents passive shear strengthening, whereas, unbonded prestressed CFRP straps provide active shear strengthening, nevertheless, the practical application of the latter can be challenging [13,14]. Alternatively, innovative iron-based shape memory alloys (Fe-SMA) have demonstrated potential in active strengthening, given their excellent strain recovery called shape memory effect. Application of prestressing with Fe-SMAs is relatively easy, as it does not involve conventional hydraulic jacks and associated end anchorages [15].

This research study presents the behaviour of prestressed concrete bridge I-girders strengthened in shear using Fe-SMA shear reinforcement in the form of plain strips or ribbed rebars. The strips were wrapped around the cross section in a rectangular way and mechanically fixed to the top of the cross section. The rebars were near surface mounted (NSM), considering a rectangular configuration, inside grooves cut around the cross section and embedded using mortar. Five I-girders have been tested to study the two shear strengthening systems, as well as the effect of activation of the Fe-SMA shear reinforcement in comparison to a similar passive (non-activated) configuration. The obtained results have been further verified against truss analogy for shear design, considering the shear contributions of the supplementary Fe-SMA shear reinforcement.

2. Shape memory alloys for active shear strengthening

Shape memory alloys (SMAs) are materials that have an intrinsic capability of recovering large deformations on heating, referred to as the shape memory effect. This relates to the phase transformation of the basic crystal structure of the material from austenite to martensite and back to austenite. In Fe-SMA, on application of the stress at ambient temperatures, austenite transforms to (mechanically induced) martensite, where, the lattice is distorted with temporary reorganization of the atoms and the phenomenon is called forward transformation (recoverable strains). The reverse transformation from martensite to austenite takes place by increasing temperature (using some form of heating method, such as resistive heating, induction heating or direct heating using a gas flame). Forward transformation to some extent also induces plastic deformations, thus, all the deformations in the SMA cannot be recovered during the reverse transformations. The temperature range for phase transformation (both reverse and forward) depends on the constituent metals of the SMA. A detailed discussion of martensitic transformation in Fe-SMA in comparison to Ni-Ti SMA can be found in [16].

There are various types of SMAs that have been researched for strengthening civil engineering structures, for example nickel titanium (Ni-Ti) [17], nickel titanium niobium (Ni-Ti-NB) [18,19], copper aluminum manganese (Cu-Al-Mn) [20] and iron-based SMAs [21–24]. The latter type, that is Fe-SMA, has been specifically designed at Empa [25] and is believed to be most suitable with respect to the application costs and ambient conditions of civil engineering structures. Because of the high iron content, Fe-SMA lacks superelasticity, though shows a reasonable strain recovery up to 1% (compared to 6–8% for NiTi-SMA) and a recovery stress of approximately 300 MPa, if heated to 200^{o}C and cooling down to the room temperature. Another notable property of Fe-SMA is very high ductility i.e. elongations up to 25–30% at failure, thus if used as shear reinforcement can help in achieving ductile shear behaviours. Detailed characterization of Fe-SMA has been reported in literature, with focus on phase transformation [26], stress recovery [27,28] and mechanical performance [29,30].

If a pre-strained SMA strip or rebar is anchored at the ends against a structural member, followed by heating, a reverse transformation takes place resulting in the application of prestress on the structure. Nearly two decades ago, the first laboratory demonstration used pre-strained Fe-SMA rods anchored onto the damaged structural elements to restore integrity by application of counteracting forces, and this concept was later applied to a real scale bridge for shear strengthening [21]. Subsequently, the interest in Fe-SMA for strengthening of concrete structures gradually increased. The use of SMA as shear reinforcement has been initially studied at small scale ‘proof of concept’, that used Ni-Ti wire spiral as internal shear reinforcement in various configurations utilizing pseudoelasticity at ambient temperatures in order to achieve ductile shear failures [17]. Another study used activated internal Fe-SMA stirrups in comparison to passive counterparts, reporting 8% increase in shear strength of the reinforced concrete beams with reduced shear cracking, also verified with numerical analysis [31]. Ni-Ti-Nb wires in a small scale study [18], wrapped around the cross section of rectangular beams as external activated reinforcement, exhibited 90 to 115% increase in shear strength of the retrofitted beams with more ductile shear failures. The use of Fe-SMA strips as shear strengthening of existing members has been demonstrated for small scale T-beams [32] by anchoring the U-shaped strips into the top web part of the beams using mechanical anchors. According to the authors, the test results were not conclusive as in few of the tests, the adapted anchorage system proved to be inefficient, when the shear cracks passed through the anchor regions leading to local failure of the concrete. However, for the remaining tests with different number of Fe-SMA strips the positive effect of active shear strengthening was demonstrated. Another similar study [33] used Fe-SMA U-shaped strips on relatively larger T-beams anchored mechanically into the web, and reported a 30% increase in shear capacity compared to the control specimen with delayed shear cracking in the activated specimens. However, the same problem of local failure of the anchorage zone as reported in [32] was also observed in this study. The same research group, carried out another experimental campaign [34] applying Fe-SMA strips as shear reinforcement on small scale rectangular beams with a different anchorage system based on buckle and shot nail. However, realization of such an anchorage system for real scale applications is challenging, as it is not very easy to bend

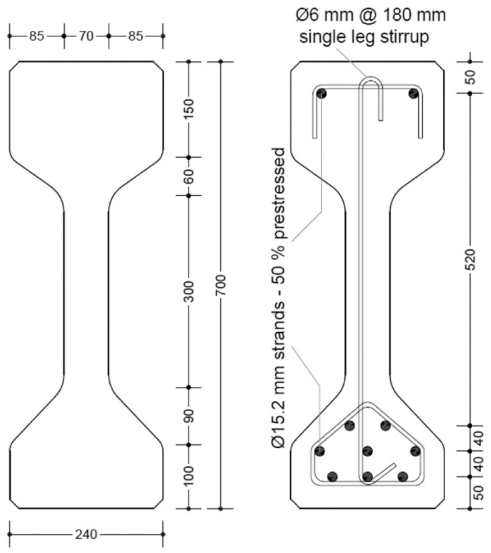

Fig. 1. Cross section and reinforcement details of PC I-girder (mm).

relatively thick Fe-SMA strip across the buckle, while, this test campaign being on small scale used only 0.5 mm thick Fe-SMA strips. These experimental results were further validated by means of a numerical model [35].

At Empa Switzerland, Fe-SMA stirrups in the form of U-shaped ribbed bars were used in combination with sprayed mortar for shear strengthening of reinforced concrete T-beams with a height of 0.75 m and a total length of 5.2 m [22]. The Fe-SMA bars were activated using electric resistive heating, resulting in vertical compressive stresses in the web of the RC beams. Subsequently, experiments were performed to show the practicability and effectiveness of this shear strengthening configuration. It was concluded that the shear capacity could be increased significantly, up to 70–86%. Furthermore, at serviceability limit state, the prestressed Fe-SMA stirrups reduced the overall beam deflections, the stresses in the internal steel stirrups, the number as well as width of the cracks [22]. Further to shear strengthening, various other strengthening interventions using SMA materials are documented in the research literature, for example flexural strengthening of beams [23,24,36,37], confinement of columns [19,38], strengthening of beam-column joints [39,40] and bond behaviour [41,42]. State-of-the-art use of SMAs in civil engineering can also be found in [15,16,43–45].

The significance of this research is to assess active shear strengthening solutions, using Fe-SMA (strips or rebars) for PC I-girders, whose cross section is difficult to strengthen in shear. In contrast to the available limited scale studies, this research utilizes full-scale specimens for assessing the potential of Fe-SMA for strengthening large structures such as concrete bridges.

3. Materials and methods

The experimental design constituted of five shear tests on 10 m long PC I-girders strengthened in shear using Fe-SMA strips or rebars. The first specimen was the reference (control), and the remaining four specimens were shear strengthened, in order to assess the potential of memory steel for active shear strengthening. After the application of the shear strengthening systems, the girders were monotonically loaded until failure. The experimental program was designed to study the effect of two different shear strengthening systems (externally applied Fe-SMA strips and near surface mounted Fe-SMA rebars) in two different ways (passive and active).

3.1. Test specimens

PC I-girders with a length of 10 m were ordered at a precast plant. The specimens were designed specifically to fail in shear even with supplementary Fe-SMA shear reinforcement, hence providing substantial margin for shear strengthening without achieving flexural failure. A typical cross section of precast PC I-girders was selected as shown in Fig. 1. The I-girder cross section has a height of 700 mm with a total width of 240 mm at both top and bottom flanges and 70 mm at the web. The longitudinal reinforcement details include eight Ø 15.2 mm strands in the tension region and two Ø 15.2 mm strands in the compression region. All these strands were prestressed to 50% of their design tensile strength (930 MPa). This rather atypical prestress value allowed the accommodation of additional flexural reinforcement needed for the ultimate limit state while maintaining the acceptable strain values at the service load conditions and to compensate for the special test configuration shown later in Fig. 7. The shear reinforcement consisted of Ø 6 mm single leg stirrups placed alternating at a spacing of 180 mm. These test specimens were cast at a precast factory located in Lier Belgium, where they were kept for curing until one month. After this curing period, the specimens were transported to Magnel-Vandepitte Laboratory at Ghent University Belgium, for installation of the Fe-SMA shear strengthening systems and testing.

3.2. Strengthening configurations and test preparations

The strengthening of I-girders employed Fe-SMA shear reinforcement in two different forms i.e. strips and rebars. The first shear strengthening system was based on Fe-SMA strips provided as externally applied reinforcement (EAR) in closed rectangular configuration,

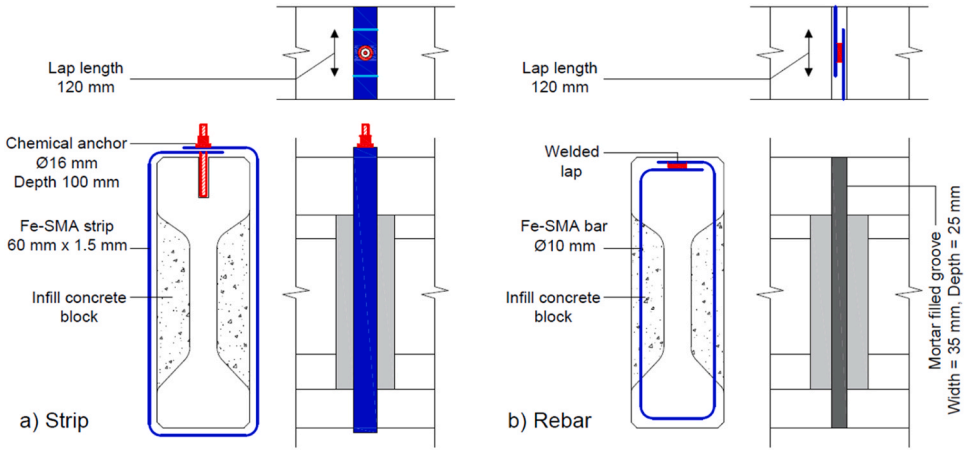

Fig. 2. Fe-SMA shear strengthening configurations using a) strip and b) rebar.

Table 1
Specimen designations.

Designation	Fe-SMA	Activation	Mode	Anchoring
Control	-	-	-	-
I-Sp	Strips	Passive	EAR	Chemical anchors
I-Sa	Strips	Activated	EAR	Chemical anchors
I-Bp	Rebars	Passive	NSM	Weld
I-Ba	Rebars	Activated	NSM	Weld

anchored on the top using chemical anchors as shown in Fig. 2a. The second shear strengthening system was based on Fe-SMA rebars provided as near surface mounted (NSM) reinforcement in closed rectangular configurations, that were welded at the top and embedded in a groove using mortar as shown in Fig. 2b. Two specimens for each shear strengthening system were prepared in a similar way, of which only one specimen was activated. An overview of specimen designations and characteristics is given in Table 1.

The anchoring of Fe-SMA strips and Fe-SMA rebars around the cross section of the I-girder is not so easy and requires careful consideration while designing a shear strengthening system. The anchoring system should be capable of developing maximum tension in the Fe-SMA without local failure of the anchors. In case of I-girders, anchoring of Fe-SMA strips to the compression flanges is not desirable because of the limited depth of the flanges, which are susceptible to local failures. Similarly, in case of rebars, there should be enough bond overlap length available for anchoring, that is limited to the top flange dimensions. Before executing this full scale study, two small scale studies were carried out by the authors to access the performance of the end conditions of externally applied Fe-SMA strips and NSM Fe-SMA rebars on concrete I-sections. In the first study with Fe-SMA strips [46], it was concluded that limited width of flanges were not able to withstand the prestress force from the Fe-SMA strips and local failure in the concrete was observed. However, when the Fe-SMA strips were anchored over the top

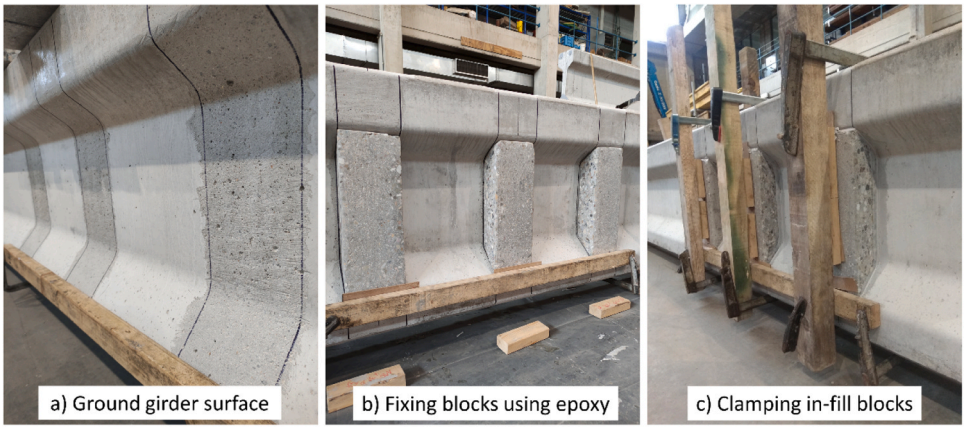

Fig. 3. Transformation of the I-section into rectangular section.

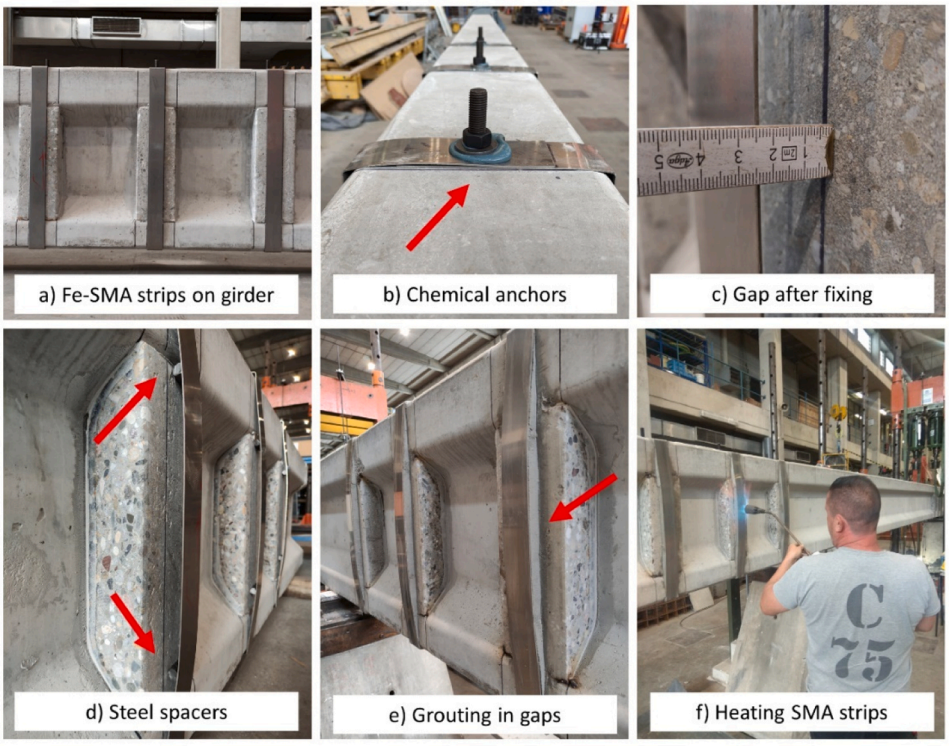

Fig. 4. Preparation of specimens with EAR Fe-SMA strips.

Fig. 5. Preparation of specimens with NSM Fe-SMA rebars.

of the I-sections in a closed configuration, it showed exceptional anchorage behaviour under loading. The second study with Fe-SMA rebars [47] reported premature failure of the specimens, when the short bends at the ends of the Fe-SMA rebar stirrups were pulled out before yielding. Based on these observations, for the current study, it was decided to anchor the strips as well as the rebars in a closed configuration (by chemical anchoring or welding, respectively).

The I-shape was transformed to an equivalent rectangular shape with epoxy bonded in-fill concrete blocks, locally at the position of Fe-SMA shear reinforcement. The concrete blocks were cast in the lab, using molds following the contours of the I-girder and the curing was carried out for a month. Afterwards, the blocks were cut to a width of 150 mm and their contact surface was prepared for epoxy bonding by grinding. The surface of the I-girder was also ground in a similar way to remove the cement laitance (Fig. 3a). Thixotropic two component epoxy adhesive [48] was used for bonding the in-fill concrete blocks (Fig. 3b). The blocks were pressed against the web of the I-girder using temporary clamps (Fig. 3c), that were removed after 12 h, while the epoxy adhesive was given 7 days to cure.

The preparation of specimens with Fe-SMA strips involved several steps as shown in Fig. 4. The Fe-SMA strips were pre-bend to the desired shape and installed around the cross section (Fig. 4a). Over the top, the strips have an extra length providing a lap of 120 mm (Fig. 2a). The holes were drilled on the top of the I-girder to a depth of 100 mm and Ø 16 mm threaded high quality steel bolts were fixed using chemical anchoring technique (Fig. 4b). Fixing of the Fe-SMA strips was a challenge in order to avoid gaps around the cross section. This problem is also identified in [33,34] for small and large scale beams respectively. In order to achieve efficient recovery stress while activating Fe-SMA, there should not be any gaps between the concrete and the Fe-SMA strips. The possibility of having gaps between the Fe-SMA strips and the concrete cross section increases as the size of cross section to be strengthened increases, hence, it is a critical concern in case of strengthening bridge girders with Fe-SMA strips. Nevertheless, after fixing the strips on the top of I-girder, a 10 – 30 mm gap was observed at the mid height on either side of the I-girders (Fig. 4c). To resolve this issue, temporary steel spacers were put behind the strips (Fig. 4d) and the gap was filled with high strength mortar (Fig. 4e). After curing the mortar for three days, the Fe-SMA strips were activated using gas flame for the specimen I-S-a (Fig. 4f). Resistive heating cannot be applied for the closed Fe-SMA strengthening configurations as used in this experimental program, therefore, gas flame had been employed that is also widely used for activation of Fe-SMA in commercial applications. The activation temperature of Fe-SMA was 160 °C, however, the heating was continued till the temperature of the Fe-SMA strips reached 300–350 °C, to eliminate the effect of non-uniform gas heating across the full length of Fe-SMA strip (except the top). The temperature during the heating process was monitored using infrared thermometer.

The steps undertaken for the preparation of the specimens with Fe-SMA rebars are shown in Fig. 5. As a first step, grooves of nominally 35 mm width and 25 mm depth were cut around the transformed rectangular periphery of the I-girder (Fig. 5a) and were shaped with chisel and hammer (Fig. 5b). Afterwards, Fe-SMA rebars were bent in rectangular shape with a lap of 120 mm on the top (Fig. 2b). The bars were installed inside the groove and the lap at the top was welded (Fig. 5c) followed by grouting only in the flange zones at the top and the bottom (Fig. 5d). The grooves were kept open at the sides, so to allow for the activation of specimen I-B-a (Fig. 5e). After activation (similarly done as described before) and bonding strain gauges on the Fe-SMA rebars, wooden form was fixed over the grooves to completely embed the Fe-SMA rebars in the mortar (Fig. 5f).

The lap on the top of Fe-SMA strip anchored using a single bolt in the middle provided concentric anchorage that cancels out the forces in the opposite directions. The anchor bolt should be capable of resisting double shear applied by the Fe-SMA strips. The welding of Fe-SMA rebar lap involves heating that can trigger early shape recovery of Fe-SMA rebars before actual anchoring. However, careful monitoring during the welding process showed that the heating effect was limited in the region of the top bend only and has no severe impact on the early shape recovery of rest of the length of the Fe-SMA rebars. It should be noted that anchoring of Fe-SMA strips and rebars as used in this study, is quite practical for the on-site applications, requiring drilling of holes and cutting of grooves through the deck slab to accommodate the anchorage laps of Fe-SMA stirrups, that can be easily embedded in the deck slab.

It should be noted that for each specimen, three Fe-SMA strip/rebar stirrups were provided at centre to centre spacing of 450 mm, equally distributed over the shear span of 1800 mm as shown schematically later in Fig. 8. In order to have a correct comparison between the two systems, the strip and the rebar cross-sectional area should be equal. The Fe-SMA rebar with nominal Ø 10 mm applied has a cross-sectional area of nearly 90 mm^2, so the width of the Fe-SMA strips was cut to have an equivalent area, by considering 60 mm width with a thickness of 1.5 mm. After the

Table 2
Strength of reference test specimens at the time of large-scale shear tests.

Concrete for casting	Compressive strength (MPa)	Flexural tensile strength (MPa)	Splitting tensile strength (MPa)
PC I-girders	101.6	4.5	4.0
In-fill blocks	58.3	6.6	4.4

Table 3
Mechanical properties of steel and Fe-SMA reinforcement.

Reinforcement type	Nominal size (mm)	Yield strength * (MPa)	Tensile strength (MPa)	Ultimate strain (%)	Elastic modulus (GPa)
Strands	Ø 15.2	1725	1970	5.3	200
Stirrups	Ø 6.0	590	633	4.3	200
Fe-SMA Rebars	Ø 10.7	520	775	26.0	110
Fe-SMA Strips	60 × 1.5	650	980	28.0	70
Threaded bars for external stirrups	Ø 16.0	670	800	4.0	200

* 0.2% proof stress.

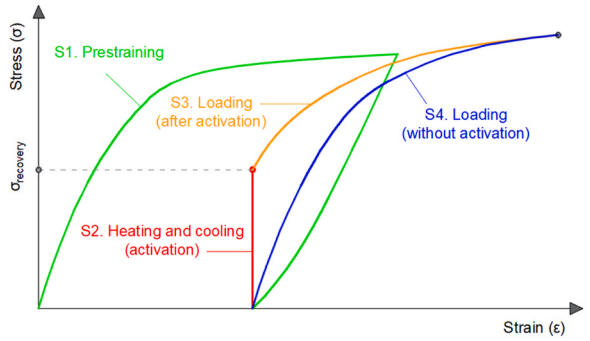

Fig. 6. Schematic illustration of mechanical behaviour of Fe-SMA reinforcement.

activation, a prestress of approximately 380 MPa was expected in Fe-SMA strips [49] and 400 MPa was expected in Fe-SMA rebars [50], when heated up to 300–350 °C using a gas flame, resulting in a prestressing force of approximately 34 kN and 36 kN in each leg of a stirrup, respectively.

3.3. Material properties

The concrete properties are given in Table 2. For casting of the PC I-girders at the precast factory, high strength self-compacting concrete was used with a maximum aggregate size of 16 mm (crushed aggregates). While, the in-fill concrete blocks were cast at the laboratory, using a normal strength concrete mix also with a maximum aggregate size of 16 mm (round aggregates). Quality control cubes and prisms were cast alongside for verification of concrete strength. The age of the I-girders (and the quality control specimens) was roughly 9 – 10 months, while, for the in-fill concrete blocks, this was around 4 – 5 months, at the time of conducting the shear tests. The test values for the compressive strength (average of 3 cubes with side length 150 mm tested according to NBN EN 12390–3), flexural and splitting tensile strength (average of 3 prisms of 150 ×150×600 mm^3 for PC I-girder and 100 ×100×400 mm^3 for in-fill blocks, tested according to NBN EN 12390–5 and NBN EN 12390–6) are given in Table 2.

The mechanical properties of prestressing strands, steel stirrups, Fe-SMA rebars (tested according to NBN EN ISO 15630–19) and Fe-SMA strips (dog bone specimens, tested according to ASTM E8) are reported in Table 3. The stress strain behaviour of Fe-SMA is highly non-linear, therefore, 0.2% offset yield criterion was used to define the yield strength and elastic modulus was defined by a straight line intersecting stress-strain curve at two points i.e. 0.2 and 0.5 of the ultimate strength of Fe-SMA.

The Fe-SMA used for this study had a composition of Fe-17Mn-5Si-10Cr-4Ni-1(V,C) (mass%) [25]. In Fig. 6, various steps involved in using Fe-SMA reinforcement are defined over the tensile stress-strain (σ-ε) diagram, indicated as 'S1 to S4'. To attain recovery stress, Fe-SMA is prestrained at first (S1) up to 2% and 4%, respectively for strips and rebars. In this study, this was done by the manufacturer before delivery of the material. For the activated specimens (I-Sa and I-Ba), Fe-SMA reinforcement after prestraining (S1) followed activation (S2) and loading (S3), whereas, for passive specimens (I-Sp and I-Bp), prestraining of Fe-SMA reinforcement (S1) directly followed loading (S4). The later scenario is not intended for Fe-SMA usage in reality, however, for this experimental program it served as a reference to observe the influence of activation on the shear behaviour. The results of Fe-SMA reported in Table 3 relate to tensile test coupons that have been previously prestrained and without activation (corresponding to the part S4 in Fig. 6).

3.4. Test setup and instrumentation

The test setup, as given in Fig. 7, was designed in such a way that two tests can be performed on one PC I-girder (one test at both girder ends, except for the control girder that was tested only on one end). During the first test, 2.48 m was kept overhanging over the support away from the load, to ensure that the shear span for the second test stays out of the influence of the load applied during the first test. Here, the first test refers to the passive (non-activated) Fe-SMA configuration, while the second test on the same beam refers to the similar activated Fe-SMA configuration. For all the tests, a shear span to effective depth ratio of 2.93 was used (a/d_e=1800/615). A straight line connecting the edge of the support plate to the edge of the loading plate has an inclination of 23°. The zone in between the two test regions was additionally strengthened (for testing reasons) using Ø 16 mm high strength threaded bars fixed with steel channel sections at a spacing of 500 mm. This external strengthening restricted the shear crack openings in this region, although shear loads are relatively limited in this longer shear span, they slightly exceeded the shear cracking load. The loading during the test was applied by two hydraulic jacks of capacity 500 kN each, fixed to the

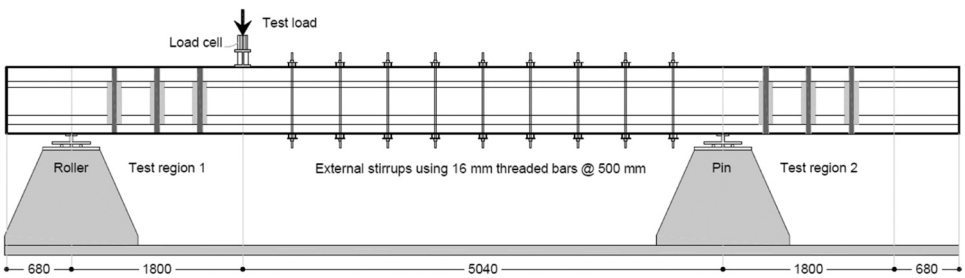

Fig. 7. Test setup (dimensions in mm).

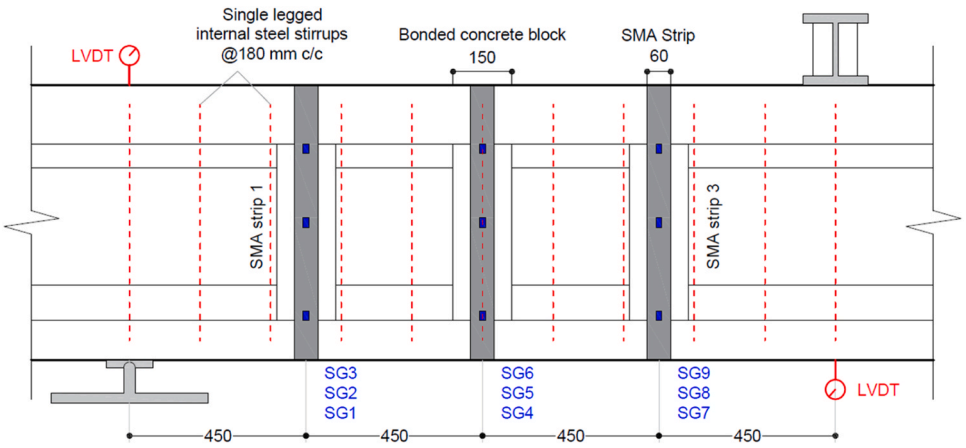

Fig. 8. Detail of instrumentation used (the same configuration applies for the both strengthening systems).

Table 4
Ultimate loads and deflections.

Specimen	Load at first shear crack (kN)	Ultimate load (kN)	Ultimate shear (kN)	Crack angle (°)	Increase in ultimate load/ shear (%)	Displacement at ultimate load (mm)	Increase in displacement (%)
Control	337	519	383	20	-	20	-
I-Sp	375	727	536	25, 32	40	42	109
I-Sa	389	734	541	26, 30	41	40	99
I-Bp	384	759	560	23, 34	46	42	112
I-Ba	384	766	564	29, 34	47	45	128

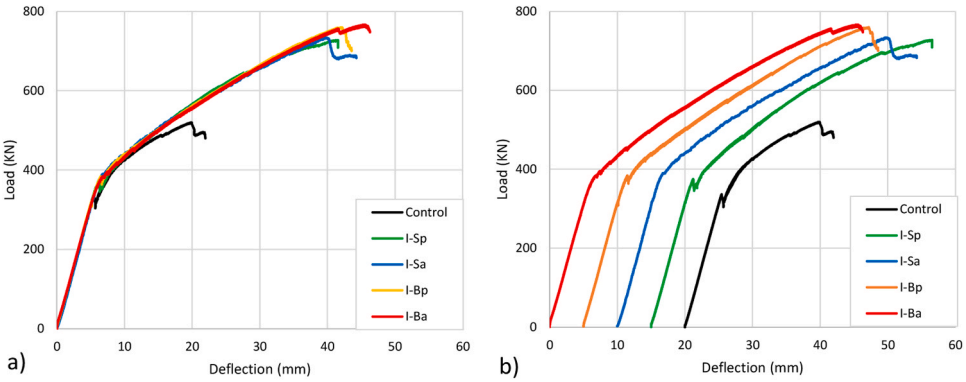

Fig. 9. Load deflection curves at a) origin b) an offset of 5 mm.

reaction frame and positioned next to each in a lateral way. The load is applied to the specimen in a displacement controlled way at a rate of 0.4 mm/minute, via a steel profile (HEM-160) and recorded by load cells.

The behaviour of each test specimen up to failure load was continuously recorded using various sensors as shown in Fig. 8. Two load cells (capacity 500 kN each) were used to record the load applied by the hydraulic jacks. The displacement under the load and over the supports was recorded using linear variable differential transformers (LVDTs). Local strain measurement in the Fe-SMA strips and rebars was

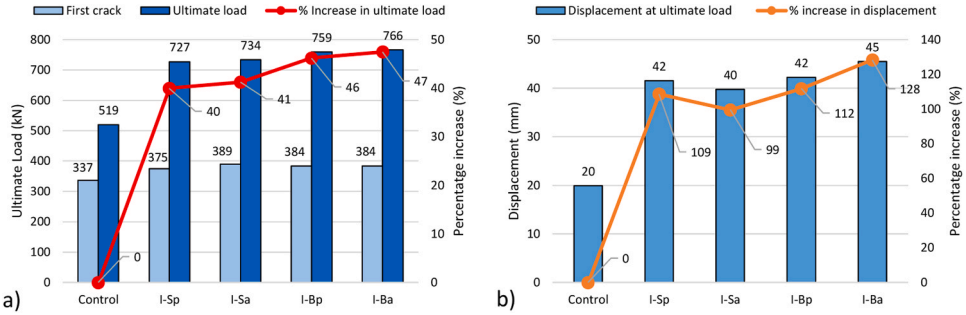

Fig. 10. Comparison of Ultimate loads and deflections.

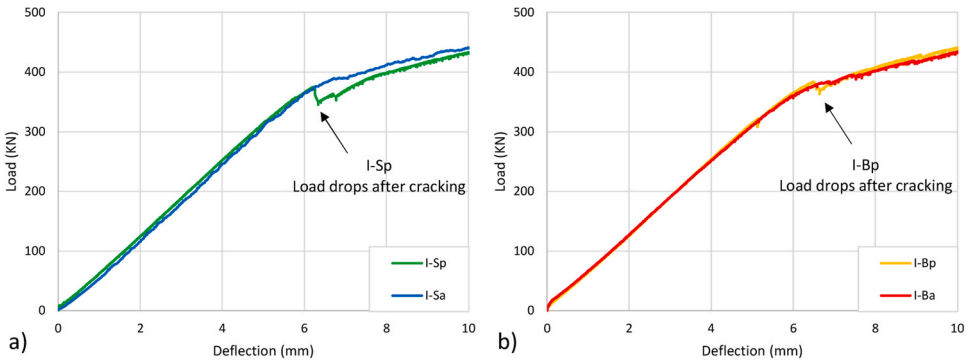

Fig. 11. Load-deflection curves up to first shear cracking a) specimen with Fe-SMA strips b) specimens with Fe-SMA rebars.

carried out by three strain gauges bonded to each strip/rebar, thereby, a total of 9 strain gauges were used for each test as named (SG1 – SG9) and positioned in Fig. 8. For observation of the full shear span, digital image correlation (DIC) measurements were carried out on the side opposite to that of the strain gauges.

4. Experimental results

The observations made during the experiments are given in the following sections, in terms of load-deflection behaviour, ultimate load, failure mode, shear crack development and the corresponding strain variation in the supplementary Fe-SMA shear reinforcement. A summary of the main test results is given in Table 4.

4.1. Load-deflection behaviour and ultimate loads

The plot of load versus deflection under the point of loading is shown in Fig. 9a. As all the load-deflection curves are nearly coincident, for better illustration another plot is shown in Fig. 9b, where, the load-deflection curves are plotted at an offset of 5 mm for each test. The values of the load at first shear crack, ultimate load, corresponding displacements and crack angle along with the effect of strengthening in terms of percentage increase in load and displacement is listed in Table 4. Graphical representation of the tabulated values are also given in Fig. 10.

It can be seen that all shear strengthening configurations helped in increasing the shear capacity, with very similar strengthening degrees of 40 to 47%, as depicted in Fig. 10a. The specimens I-Sp and I-Sa exhibited an increase in shear strength of 40% and 41%, respectively. Likewise, the specimens I-Bp and I-Ba exhibited an increase in shear strength of 46% and 47%, respectively. Given the higher capacity, the deflection at ultimate load of the strengthened specimens was more than double, compared to the control specimen, as shown in Fig. 10b.

Fig. 11a shows the load deflection curve up to 10 mm for specimen I-Sp and I-Sa, where it can be seen that for both the specimens, service load behaviour is almost the same. A similar observation was also made for specimens I-Bp and I-Ba in Fig. 11b. It can be concluded, that up to service load level (before shear cracking) there is no obvious increase in the stiffness of the specimens with activated Fe-SMA shear reinforcement. However, there is a clear difference at the point of first shear cracking, where the specimens without activation showed sudden load drop compared to the activated specimens that exhibited smooth transition from elastic to nonlinear zone.

The effect of transverse prestress applied by the activation of Fe-SMA as well as epoxy bonded in-fill concrete blocks, in comparison to the control can be investigated with respect to the emergence of the first shear crack (as visually observed during the experiment and the point at which the load deflection curve changes slope). For each test, load at first shear crack is listed in Table 4 and comparatively shown in Fig. 10a. The load values at the first shear crack for the specimen I-Sp and I-Sa is 375 kN and 389 kN, respectively. Similarly, for specimen I-Bp and I-Ba, the values at which first shear crack was observed is similar for both the tests i.e. 384 kN. Since there is no significant difference between the activated and the passive specimens, as the shear cracking started in the same order of load magnitude, it can be inferred that the magnitude of the Fe-SMA prestress was not enough to delay the shear cracking significantly in the activated specimens. However, these load values of first shear cracking for strengthened specimens are slightly higher than that of control test i.e. 337 kN. This range of difference in loads, 38 – 52 kN (minimum and maximum) in terms of delay in shear cracking can be linked to the presence of epoxy bonded in-fill concrete blocks that provided additional concrete cross section across the anticipated shear cracking region. It can also be observed that the range of the ultimate loads for the strengthened specimens is almost the same, subject to an equivalent cross sectional area of Fe-SMA strips and rebars (90 mm^2) across the shear span in both the systems. The NSM system resisted slightly higher loads compared to the externally applied system subject to fully bonded Fe-SMA rebars, providing better confinement over the girder periphery.

4.2. Crack pattern and failure mode

The crack pattern at the ultimate loads visualized by means of DIC (major principle strains, $\varepsilon 1$), along with the final failure mode for each specimen is shown in Fig. 12. Failure of all the specimens started with emergence of a web shear crack at approximately mid height of the PC I-girders, which continue to develop towards the loading point and the support on further increase in the load. In case of the control specimen, the shear crack was fully developed along the shear span exhibiting the yielding of the internal steel stirrups. At the end, the failure was brittle as majority of the steel stirrups across the shear span ruptured with disintegration of concrete in the compression zone as shown in Fig. 12a.

For specimen I-Sp, the shear crack near ultimate first intersected the point of the load, immediately followed by the rupture of the Fe-SMA strip in the middle as can be seen in Fig. 12b. The Fe-SMA strip ruptured at the bend because of the stress concentration and sudden redistribution of the load at failure. In case of specimen I-Sa, failure was not governed by the main shear crack, however close to the failure, secondary shear crack (towards right) rapidly developed because of closely spaced multiple shear cracks leading to concrete compression in the top flange as seen in Fig. 12c. In this test, none of the Fe-SMA strips ruptured but concrete failed. In both the specimens I-Sp and I-Sa, no warping of Fe-SMA strips was observed near the anchor bolts. For specimens I-Bp and I-Ba brittle failure was observed, after the shear crack reached the point of loading as seen in Fig. 12d and e, respectively. During post failure observations in both of these tests, none of the Fe-SMA rebars or the welds at the laps were observed to rupture.

It can be seen that, the ultimate failure in all the strengthened specimens (except I-Ba) took place along the steep shear crack between the two Fe-SMA stirrups, indicating a weak shear plane intercepted by a

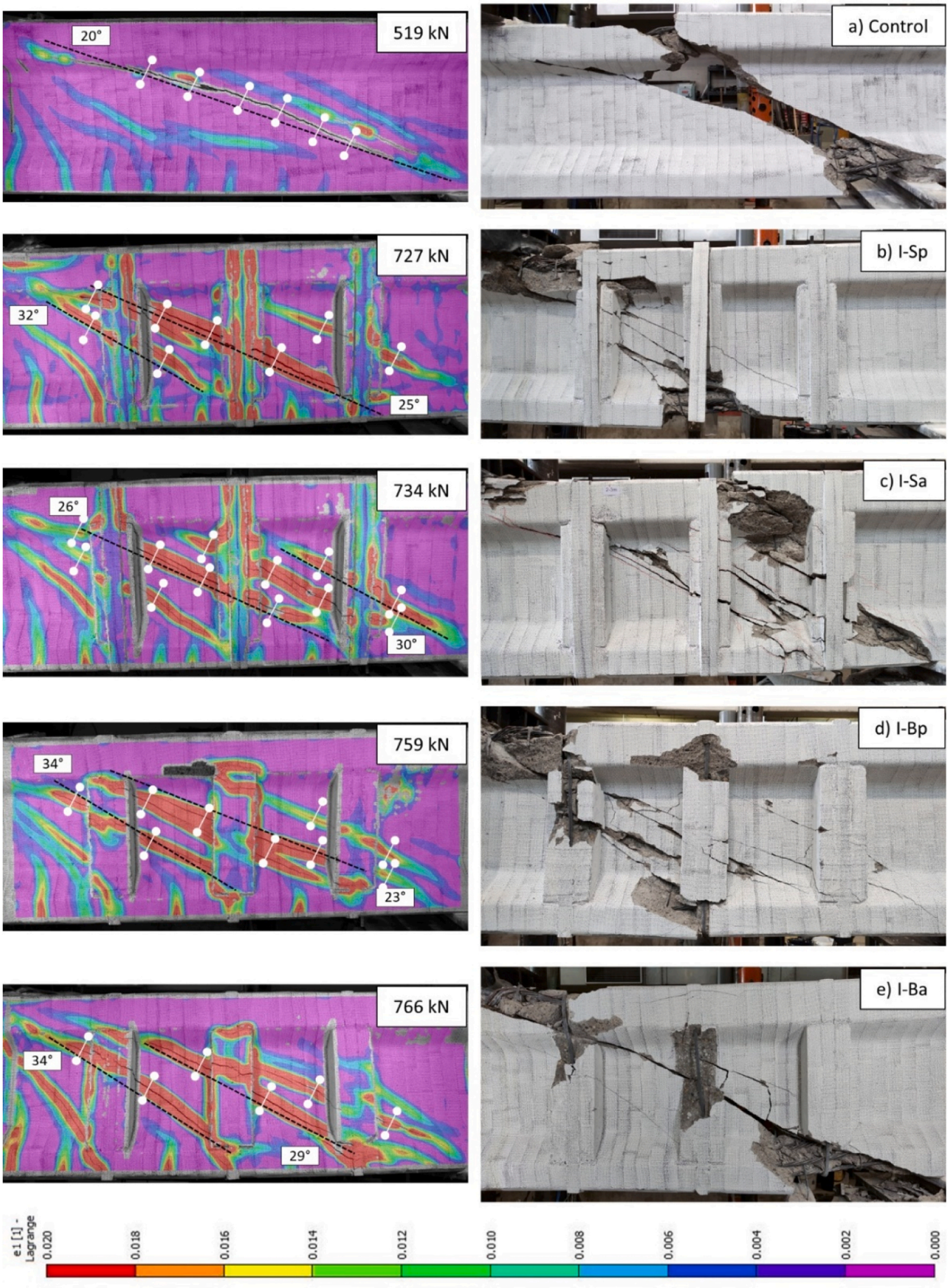

Fig. 12. Crack pattern and ultimate failure mode of specimens (white connected dots represent virtual extensometers for crack opening, colour legend represent principal strains, unit = mm/mm).

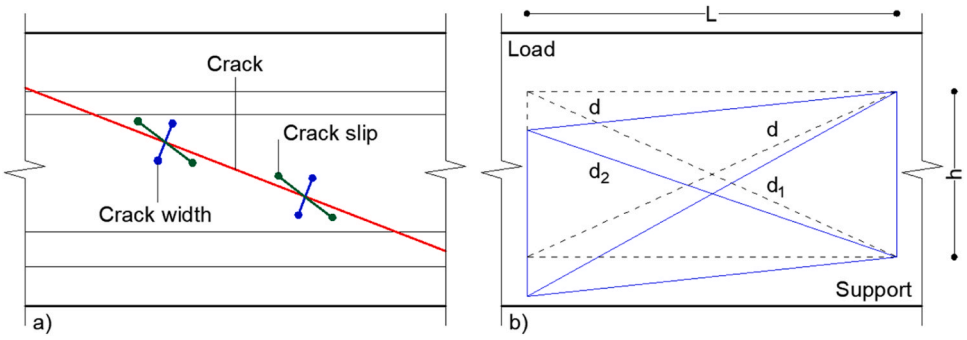

Fig. 13. Virtual sensors used in DIC analysis for measuring a) crack width and slip b) shear strain.

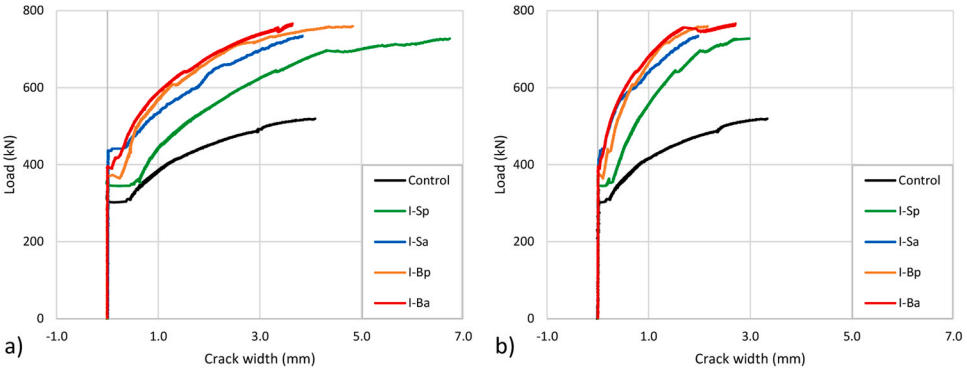

Fig. 14. Progression of shear crack width a) maximum b) average.

less number of steel and Fe-SMA stirrups. Well distributed shear cracking was observed (Fig. 12, left) in the shear span of all the strengthened specimens, where, shallow primary shear cracks being fully arrested by almost all the Fe-SMA stirrups couldn't open but relatively steep secondary shear cracks took over to failure. The inclination of all the shear cracks are indicated by black dotted lines in Fig. 12 and the values of the main shear crack angles are listed in Table 4. The range of shear crack angle was between 20 to 34 degrees, that is in line with the shear provisions of Model Code 2010 [51] for prestressed concrete beams. The shear crack angle of the strengthened specimens was on average 29 degrees (i.e. 45% higher than the reference).

A limited number of flexural cracks also appeared in all of the tests as can be seen from the DIC observations in Fig. 12. For all the tests, the shear cracking in the web and the epoxy bonded in-fill concrete blocks took place at the same instant and the same locations, depicting a perfect bond between web and the in-fill concrete blocks.

4.3. Shear crack width and slip

The increase in load after emergence of the shear crack, increases the crack width and the crack plane slips with gradual receding of the aggregate interlocking. Both of these quantities (crack width and crack slip) were measured for all the tests using DIC measurements. Virtual extensometers were placed perpendicular to the major shear cracks to measure the crack width and similar extensometers were placed (nearly) parallel to the major shear cracks at two points along the crack length as shown schematically in Fig. 13a. The maximum and average crack width measured with respect to the load is shown in Fig. 14, and the location of virtual extensometers with respect to the shear cracks is shown over Fig. 12 (only the extensometers perpendicular to the crack are shown).

It can be seen in Fig. 14, that the maximum or the average crack width for all the strengthened specimens become equivalent to that of the control specimen at much higher loads showing the strengthening

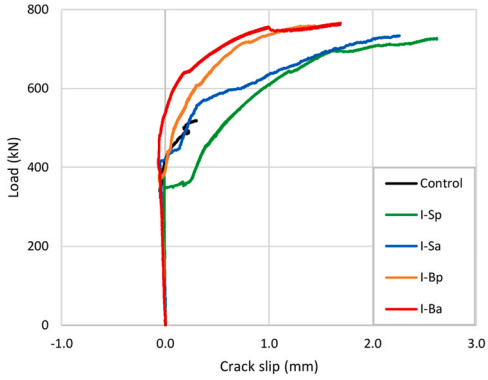

Fig. 15. Progression of shear crack slip.

effect of Fe-SMA shear reinforcement. A comparison of specimen I-Sp and I-Sa clearly shows that the crack width in the passive specimen was larger than in the activated specimen. In case of specimens I-Bp and I-Ba, this was less pronounced as the crack width increased almost identically. Nevertheless, close to the failure the passive specimens showed larger crack openings compared to the activated specimens. It can also be observed in the passive specimens that the crack widths are greater for Fe-SMA strips compared to that of Fe-SMA rebars. This is due to the difference in the applied configurations where the Fe-SMA strips being unbonded (or externally anchored) allowed for greater crack openings compared to the Fe-SMA rebars which were closely bonded as near-surface mounted reinforcement.

The virtual extensometers used for the measurement of crack slip were placed parallel to the compression strut, therefore in Fig. 15, initially before the shear cracking, the crack slip curves showed slightly negative trend indicating the compression in the shear strut. After shear cracking, the crack started to slip earlier in the passive specimens

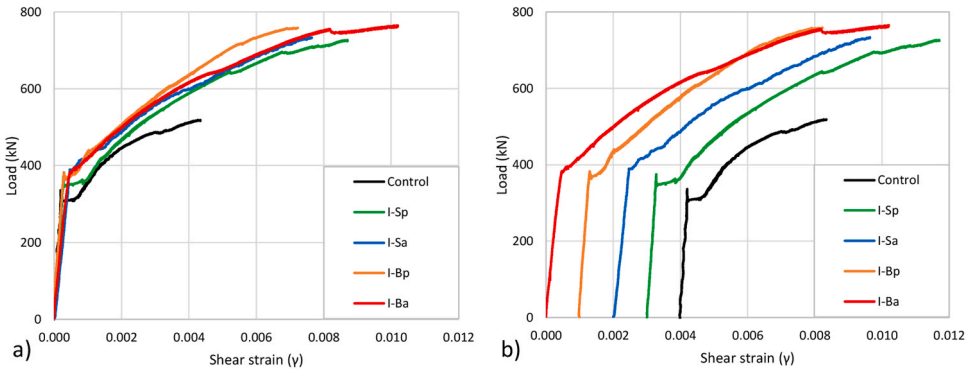

Fig. 16. Shear deformation response at a) origin b) offset of 0.001 (units for γ = mm/mm).

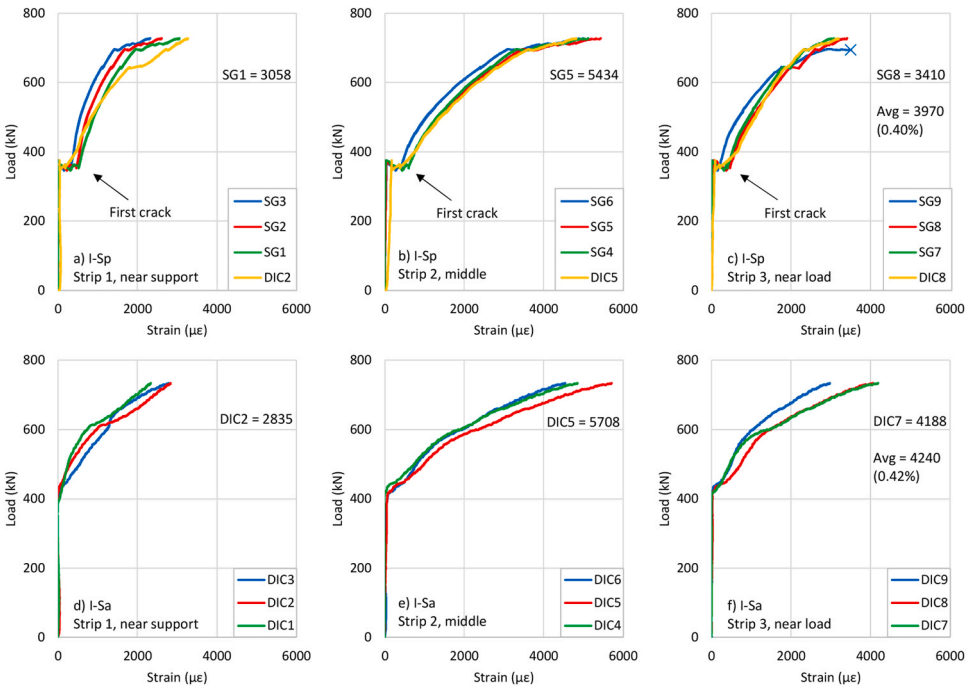

Fig. 17. Strain variation in Fe-SMA strips a-c) specimen I-Sp d-f) specimen I-Sa.

compared to the activated specimens. This clearly indicate active crack control by Fe-SMA shear reinforcement, where, lateral prestressing resisted shear slip, by increasing aggregate interlocking. The control specimen encountered a shallow shear crack, engaging relatively more internal stirrups, hence, exhibiting a lower slip compared to the I-Sp.

4.4. Shear deformation response

As shear deformation is more pronounced in slender beams [52] like I-girders, it is reported in this section in terms of shear strain. Fig. 13b shows the arrangement of virtual extensometers over the shear span used for the calculation of shear strains (γ) given by Eq. 1, using DIC measurements.

$$Shear \quad strain(\gamma) = \frac{(d_1 - d) \bullet d - (d_2 - d) \bullet d}{2Lh} \tag{1}$$

Where, L ($\approx$ 1100 mm) and h ($\approx$ 550 mm) are respectively, the length and height of the deformation region considered for the measurement. Fig. 16a shows the load versus shear strain development in each specimen with respect to the origin and for more clear illustration, Fig. 16b shows the same trend individually at an offset of 0.001. It can be seen that the shear strain suddenly increased (plateau after end of the linear shear strain stage) on shear cracking in the control specimen as well as in strengthened specimens without activation. While in case of activated specimens, the linear shear strain region transforms more smoothly into a non-linear region after shear cracking, depicting the effect of transverse prestress.

Another aspect observed in Fig. 16b is the difference in the shear stiffness (slope of load vs shear strain curve) of activated specimens, which is slightly less compared to the passive counterparts. This is noticeable both in the linear and the non-linear regions, however, comparatively less prominent in the linear region subject to the positive effect of prestressing of the steel strands. This difference is believed to be, due to the repetition of second shear test (activated specimens) on the same PC I-girders already tested (passive specimens) at the opposite end. During the first test, the span in between the two test regions undergoes a certain level of damage both in shear and in flexure, because of which the I-girder showed slightly lower shear stiffness during the second test. This trend can also be seen in Fig. 9b in terms of load-deflection behaviour but is comparatively less prominent.

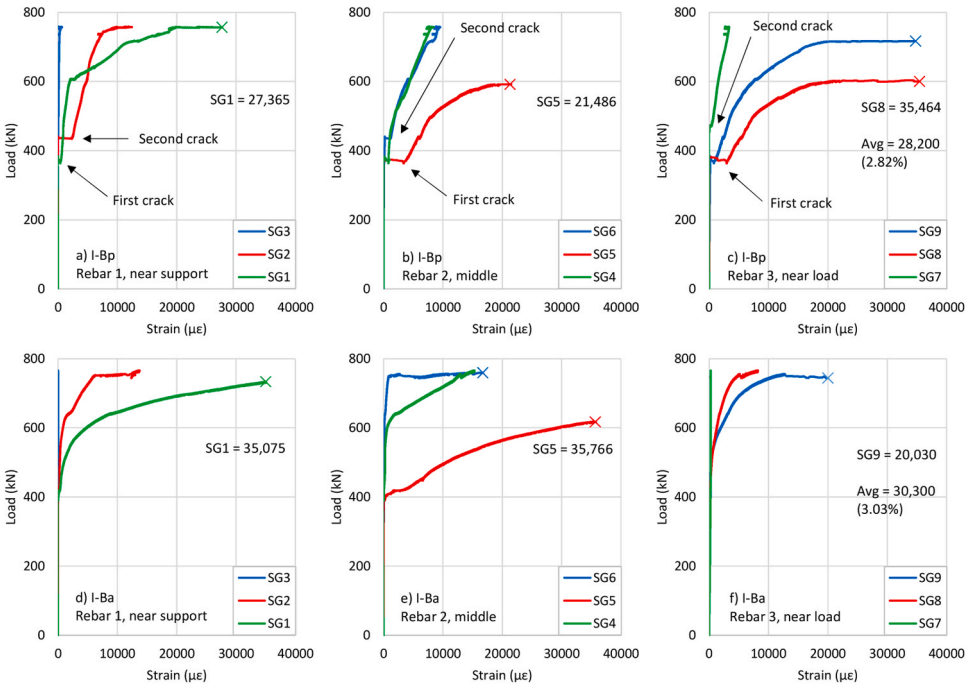

Fig. 18. Variation of strains in Fe-SMA rebars a-c) specimen I-Bp d-f) specimen I-Ba.

4.5. Strain variation in Fe-SMA shear reinforcement

The strain on each Fe-SMA strip was measured using 3 strain gauges bonded along the strip as shown in Fig. 8 and the plot of strain values with respect to the load is illustrated in Fig. 17 (cross mark at the end of a curve shows the point at which strain gauge became offscale). For specimen I-Sa, the data from strain gauges could not be recorded because of an error in the data acquisition system, therefore, the given strain trend for this test correspond to the strain measurement at the similar locations made using DIC on the opposite side of the specimen. Fig. 17a-c show the values of strain variation in each strip for specimen I-Sp, where it can be seen that just after shear cracking, all strips started to resist the shear deformations. A similar observation can also be made for Specimen I-Sa in Fig. 17d-f, with an exception that there was no abrupt strain increase at cracking as in case of specimen I-Sp, due to the presence of transverse prestress from activation of Fe-SMA shear reinforcement. The maximum strain value in each Fe-SMA strip along with their average is also shown in Fig. 17. It should be noted that the observed strain range in I-Sp and I-Sa is almost the same at failure i.e. 0.40% and 0.42%, respectively.

Fig. 18 shows the strain variation in Fe-SMA rebars for specimen I-Bp and I-Ba. The location of strain gauges in these specimens correspond to the locations shown in Fig. 8, with the difference that the strain gauges in this case were bonded to the rebars embedded inside the groove with mortar. Fig. 18a-c shows the strain variation for specimen I-Bp, where it can be seen that after shear cracking, the strain gauges only in the region of the crack responded. Later, on further loading, other strain gauges intersecting the region of second shear crack also responded. The strain gauges outside the influence of any crack showed no response until the failure. Fig. 18d-f shows similar observations for specimen I-Ba, without any abrupt strain increase after shear cracking, depicting the presence of transverse prestress from activated Fe- Fe-SMA rebars, as also observed for specimen I-Sa. The maximum strain value in each Fe-SMA rebar along with their average is also shown in Fig. 18. Similar to the specimens with Fe-SMA strips, both the specimens with Fe-SMA rebars exhibited similar strain range at failure i.e. 2.82% and 3.03% for I-Bp and I-Ba, respectively, however, the average strain is almost 7 times higher compared to that observed in Fe-SMA strips.

The difference in the behaviour of externally applied Fe-SMA strips and Fe-SMA rebars is clear from Figs. 17 and 18. The strains in the Fe-SMA strips at cracking, shows the characteristic behaviour of unbonded shear reinforcement, where, the deformations are averaged over the full length of the stirrups. In comparison, the deformations in the bonded Fe-SMA rebars are localized, only in the region of the shear crack, resulting in much higher strain magnitudes.

5. Analytical verification of Fe-SMA shear contribution

The basic truss analogy [53] as used for internal stirrups given by Eq. 2, has been applied to calculate the contribution of Fe-SMA shear reinforcement. The two main variables involved are the stress in the Fe-SMA stirrups (σ_{sw}) and the shear crack angle (θ) used to estimate the number of stirrups intercepted by the shear crack. A tentative verification based on Eq. 2 is done in the following, particularly making use of some of the experimental observations, so to provide first insights on the applicability of the truss model approach for this specific shear strengthening configuration. More work on a predictive model would be needed in the future. The Fe-SMA shear contribution is calculated considering the shear crack angles as observed during the experiments. As indicated in Fig. 12, two major shear cracks were observed in each strengthened specimen and the weak shear plane is the one with the steepest shear crack (intercepting less stirrups), thus, the larger value of the shear crack angle was considered for the calculation.

$$V_{R,s} = A_{sw}\sigma_{sw}\frac{d}{s}\cot\theta \tag{2}$$

To identify the stress in the Fe-SMA reinforcement (σ_{sw}), the corresponding σ-ε diagram should be considered for passive (non-activated) and activated specimens (Fig. 6, S4 and S2 +S3, respectively). Furthermore, if the stress level is beyond the yield point, σ_{sw} can be taken equal to the yield strength of the Fe-SMA reinforcement. As yielding of Fe-SMA rebars is quite obvious from the load-strain behaviour observed for I-Bp and I-Ba (Fig. 18), for the verification of the Fe-SMA contribution for both the specimens, σ_{sw} was considered equal to the yield strength of Fe-SMA rebars (Table 3). For the unbonded Fe-SMA strips in I-Sp and I-Sa, strain values lower than the yield strain were observed

Table 5
Estimation of Fe-SMA reinforcement contribution.

Specimen	θ	w (mm)	ε_{cr} (%)	ε_{exp} (%)	σ_{sw} (MPa)	$V_{SMA,\ Est}$ (kN)	$V_{SMA,\ Exp}$ (kN)	V_{Est}/V_{Exp}
I-Sp	32	2.98	0.52	0.40	465	183	153	1.20
I-Sa	30	1.97	0.32	0.42	500	213	158	1.35
I-Bp	34	-	-	2.80	520	189	177	1.07
I-Ba	34	-	-	3.03	520	189	181	1.04

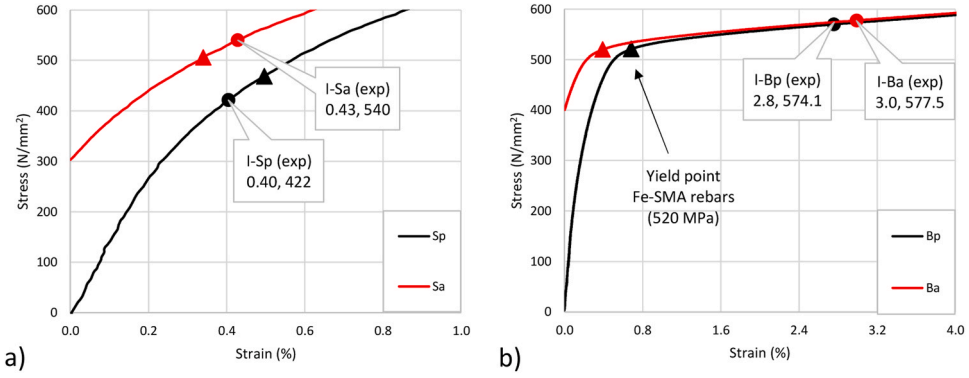

Fig. 19. Estimated versus experimental stress-strain values for a) I-S and b) I-B specimens.

(Fig. 17), therefore, σ_{sw} was estimated based on the average shear crack width observed during the experiments as given in Fig. 14b. The width of each major shear crack crossing the Fe-SMA strips was calculated perpendicular to the crack (Fig. 12), on both sides of each Fe-SMA strip and an average value was considered for the calculations. The location of virtual extensometers used for the crack width calculations are illustrated in Fig. 12 and the average values of crack width are reported in Table 5. The strain due to crack opening (ε_{cr}) was calculated using Eq. 3, where, $w/\cos\theta$ represents the projection of the crack opening in the direction of Fe-SMA strip that is divided over the full depth of Fe-SMA strip (h).

$$\varepsilon_{cr} = \frac{w}{h \bullet \cos\theta} \tag{3}$$

Using the estimated strain due to crack opening (ε_{cr}), the effective stress σ_{sw} in Fe-SMA strips can be found from the σ-ε curves as shown in Fig. 19, where the black curves starting from the origin represents the passive Fe-SMA, and the red curves starting from the recovery stress values ($\sigma_{recovery}$) represents the activated Fe-SMA. Since the recovery stress was not measured during the activation, the start of the σ-ε curve for activated Fe-SMA (i.e. 300 MPa for Fe-SMA strip and 400 MPa for Fe-SMA rebar) correspond to the recovery stress values suggested by the manufacturer and the temperature measured during the activation. Fig. 19 shows the calculated strain and the corresponding stress in Fe-SMA reinforcement using triangles, in comparison to the experimental observations highlighted as dots (see Figs. 17 and 18 for the experimental observations of strain). For specimens with Fe-SMA strips, I-Sp and I-Sa, the implemented method based on average crack width gave a reasonable estimation of strain in the Fe-SMA strips (Fig. 19a). For specimens with Fe-SMA rebars, I-Bp and I-Ba, it can be seen in Fig. 19b, that the measured strains are well beyond the yield point of Fe-SMA rebars, therefore, verification was made using the yield stress (520 MPa).

The calculation parameters and results of shear contribution of Fe-SMA reinforcement, in comparison to the experimental observations are reported in Table 5. The shear contribution of Fe-SMA reinforcement as observed in the experiments was taken equal to the difference between the shear resistance of the strengthened specimens and that of the control specimen. Although, the shear crack angle is different in the control specimen and in the strengthened specimens, the simple subtraction to find the shear contribution of Fe-SMA reinforcement still seems reasonable. This is because in all the specimens, almost the full shear span underwent multiple shear cracking, engaging all the internal stirrups, thus, in order of magnitude and for the sake of comparison an equal contribution of internal stirrups can be assumed. Finally, the ratios of estimated shear contribution (V_{Est}) of Fe-SMA reinforcement to the experimental contribution (V_{Exp}) given in Table 5, shows close estimations, except for I-Sp and I-Sa, where an overestimation has been noted. For I-Sa, this could be due to a high recovery stress value considered in the σ-ε diagram, which might be lower in reality subject to potential gaps at the bends of the Fe-SMA strips. Besides, Eq. 3 for the calculation of strain in the Fe-SMA strips is very sensitive to the shear crack inclination, as a small difference in the shear crack angle can bring a reasonable variation in the shear contribution. Hence, correct estimation of shear contribution of each component in a shear test is always challenging due to complicated interdependence of shear mechanism.

6. Conclusions

In brief, this experimental study on PC I-girders strengthened in shear using Fe-SMA reinforcement has demonstrated the following aspects.

- The design of shear strengthening systems for PC bridge I-girders requires careful consideration, as its concave shaped cross section makes it difficult to strengthen in shear.
- The presented Fe-SMA shear strengthening configurations are technically feasible with respect to both, the practical application and the efficient performance under the load.
- Fe-SMA shear strengthening (as strips or rebars) effectively applied prestress, because of its shape memory characteristics activated by heating. The Fe-SMA shear strengthening configurations in closed loops provided confinement, resulting in improved serviceability behaviour, as the activated systems in comparison to the passive (non-activated) systems proved to be beneficial for the crack width control (smaller crack widths) and for resisting the shear deformations (smaller shear deformations). However, no significant effect of prestress was observed in delaying the first shear cracking and increasing the ultimate limits.
- The externally applied shear strengthening system using Fe-SMA strips anchored at the top of the beam increased the shear strength

of tested PC I-girders up to 40 – 41%, in comparison to the control specimen. Similarly, the Fe-SMA NSM shear strengthening system increased the shear capacity of PC bridge I-girders up to 46 – 47%.

- The basic truss analogy was capable of estimating the Fe-SMA shear contribution for each test, using experimental observations on shear crack angle and stress in the Fe-SMA shear reinforcement. However, the choice of these two basic unknowns remains a challenge and a bottleneck of the shear design.

CRediT authorship contribution statement

Muhammad Arslan Yaqub: Writing – review & editing, Writing – original draft, Visualization, Validation, Methodology, Investigation, Funding acquisition, Formal analysis, Data curation, Conceptualization. **Stijn Matthys:** Writing – review & editing, Supervision, Resources, Project administration, Methodology, Investigation, Funding acquisition, Conceptualization. **Christoph Czaderski:** Writing – review & editing, Supervision, Methodology, Conceptualization.

Declaration of Competing Interest

The authors declare that they have no known competing financial interests or personal relationships that could have appeared to influence the work reported in this paper.

Data Availability

Data will be made available on request.

Acknowledgements

Special thanks goes to Pieter van der Zee (Technical Director, CRH Structural Concrete, Belgium) for his involvement in careful design of the PC I-girders followed by production and delivery to the laboratory. Secondly, Julien Michels (Managing Director, re-fer AG, Switzerland) for providing all the Fe-SMA materials used for the shear strengthening. Last but not the least, the authors are thankful to the technical staff of the Magnel-Vandepitte Laboratory, without whom the experimental tasks could never be achieved. The first author is thankful to the Higher Education Commission (HEC) Pakistan as well as Ghent University, Belgium for providing financial assistance to carry out this research.

References

[1] ARTBA, 2022 Bridge Report. 2022, The American Road & Transportation Builders Association: Washington, D.C.
[2] Hutchinson, R.L., The use of externally bonded CFRP sheets for shear strengthening of I-shaped prestressed concrete bridge girders. 2000, PhD Thesis, University of Manitoba: Canada.
[3] Kang THK, Ary MI. Shear-strengthening of reinforced & prestressed concrete beams using FRP: Part II - experimental investigation. Int J Concr Struct Mater 2012;6(1):49–57.
[4] Murphy M, Belarbi A, Bae SW. Behavior of prestressed concrete I-girders strengthened in shear with externally bonded fiber-reinforced-polymer sheets. PCI J 2012:63–82.
[5] Garcia JE, et al. Shear strengthening of concrete girders using carbon fiber-reinforced polymer sheets and anchors. Acids Struct J 2018;115(4):1165–73.
[6] Massa RJ, Cook WD, Mitchell D. Reinforcing bridge I-girders using CFRP shear strips. Acids Spec Publ 2018;328:1.1–1.20.
[7] Matthys, S., Structural behaviour and design of concrete members strengthened with externally bonded FRP reinforcement. 2000, Ghent University.
[8] Czaderski, C. Shear strengthening with prefabricated CFRP L-shaped plates. in *IABSE Symposium Report*. 2002. International Association for Bridge and Structural Engineering.
[9] Czaderski C, Motavalli M. Fatigue behaviour of CFRP L-shaped plates for shear strengthening of RC T-beams. Compos Part B-Eng 2004;35(4):279–90.
[10] Yaqub MA, Czaderski C, Matthys S. Shear strengthening of precast prestressed I-girders using carbon fiber reinforced polymers and in-fill concrete blocks. Struct Concr 2023;24(2):3091–108.
[11] Michels J, et al. Prestressed CFRP strips for concrete bridge girder retrofitting: application and static loading test. J Bridge Eng 2016;21(5).
[12] Yaqub, M.A., S. Matthys, C. Czaderski, Advancements in shear strengthening of prestressed concrete I-girders using fiber reinforced polymers, in *IABSE Congress Ghent 2021*, Structural Engineering for Future Societal Needs. 2021, IABSE, Zurich Switzerland. p. 1746–1753.
[13] Motavalli M, Czaderski C, Pfyl-Lang K. Prestressed CFRP for strengthening of reinforced concrete structures: recent developments at Empa, Switzerland. J Compos Constr 2011;15(2):194–205.
[14] Hoult NA, Lees JM. Efficient CFRP strap configurations for the shear strengthening of reinforced concrete T-Beams. J Compos Constr 2009;13(1):45–52.
[15] Janke L, et al. Applications of shape memory alloys in civil engineering structures - overview, limits and new ideas. Mater Struct 2005;38(279):578–92.
[16] Cladera A, et al. Iron-based shape memory alloys for civil engineering structures: an overview. Constr Build Mater 2014;63:281–93.
[17] Mas B, Cladera A, Ribas C. Experimental study on concrete beams reinforced with pseudoelastic Ni-Ti continuous rectangular spiral reinforcement failing in shear. Eng Struct 2016;127:759–68.
[18] Rius JM, et al. Shear strengthening of reinforced concrete beams using shape memory alloys. Constr Build Mater 2019;200:420–35.
[19] Shin M, Andrawes B. Lateral cyclic behavior of reinforced concrete columns retrofitted with shape memory spirals and FRP wraps. J Struct Eng 2011;137(11):1282–90.
[20] Araki Y, et al. Potential of superelastic Cu-Al-Mn alloy bars for seismic applications. Earthq Eng Struct Dyn 2011;40(1):107–15.
[21] Soroushian P, et al. Repair and strengthening of concrete structures through application of corrective posttensioning forces with shape memory alloys. Des Struct 2001;2001(1770):20–6.
[22] Czaderski C, Shahverdi M, Michels J. Iron based shape memory alloys as shear reinforcement for bridge girders. Constr Build Mater 2021;274.
[23] Shahverdi M, et al. Strengthening of RC beams by iron-based shape memory alloy bars embedded in a shotcrete layer. Eng Struct 2016;117:263–73.
[24] Schranz B, et al. Strengthening and prestressing of bridge decks with ribbed iron-based shape memory alloy bars. Eng Struct 2021;241.
[25] Dong ZZ, et al. A novel Fe-Mn-Si shape memory alloy with improved shape recovery properties by VC precipitation. Adv Eng Mater 2009;11(1-2):40–4.
[26] Lee WJ, et al. Phase transformation behavior under uniaxial deformation of an Fe-Mn-Si-Cr-Ni-VC shape memory alloy. Mater Sci Eng a-Struct Mater Prop Microstruct Process 2013;581:1–7.
[27] Lee WJ, et al. Stress recovery behaviour of an Fe-Mn-Si-Cr-Ni-VC shape memory alloy used for prestressing. Smart Mater Struct 2013;22(12).
[28] Lee WJ, Weber B, Leinenbach C. Recovery stress formation in a restrained Fe-Mn-Si-based shape memory alloy used for prestressing or mechanical joining. Constr Build Mater 2015;95:600–10.
[29] Michels J, et al. Mechanical Performance of Iron-Based Shape-Memory Alloy Ribbed Bars for Concrete Prestressing. Acids Mater J 2018;115(6):877–86.
[30] Shahverdi M, et al. Iron-based shape memory alloy strips for strengthening RC members: Material behavior and characterization. Constr Build Mater 2018;173:586–99.
[31] Ji S, Yeon Y, Hong K. Shear performance of RC beams reinforced with Fe-based shape memory alloy stirrups. Materials 2022;15(5).
[32] Zerbe, L., et al. Behavior of retrofitted concrete members using iron-based shape memory alloys. in Fourth Conference on Smart Monitoring, Assessment and Rehabilitation of Civil Structures. 2017.
[33] Cladera A, et al. Shear strengthening of slender reinforced concrete T-shaped beams using iron-based shape memory alloy strips. Eng Struct 2020;221.
[34] Montoya-Coronado LA, et al. Experimental study on shear strengthening of shear critical RC beams using iron-based shape memory alloy strips. Eng Struct 2019;200.
[35] Ruiz-Pinilla JG, et al. Finite element modeling of RC beams externally strengthened with iron-based shape memory alloy (Fe-SMA) strips, including analytical stress-strain curves for Fe-SMA. Eng Struct 2020;223.
[36] Shahverdi M, Czaderski C, Motavalli M. Iron-based shape memory alloys for prestressed near-surface mounted strengthening of reinforced concrete beams. Constr Build Mater 2016;112:28–38.
[37] Michels J, Shahverdi M, Czaderski C. Flexural strengthening of structural concrete with iron-based shape memory alloy strips. Struct Concr 2018;19(3):876–91.
[38] Jung D, Wilcoski J, Andrawes B. Bidirectional shake table testing of RC columns retrofitted and repaired with shape memory alloy spirals. Eng Struct 2018;160:171–85.
[39] Oudah F, El-Hacha R. Innovative Self-Centering Concrete Beam-Column Connection Reinforced Using Shape Memory Alloy. Acids Struct J 2018;115(3):607–20.
[40] Yurdakul O, Tunaboyu O, Avsar O. Retrofit of non-seismically designed beam-column joints by post-tensioned superelastic shape memory alloy bars. Bull Earthq Eng 2018;16(11):5279–307.
[41] Schranz B, et al. Bond investigations of prestressed, near-surface-mounted, ribbed memory-steel bars with full bond length. Mater Des 2020;196.
[42] Schranz B, et al. Bond behaviour of ribbed near-surface-mounted iron-based shape memory alloy bars with short bond lengths. Mater Des 2020;191.
[43] Alam MS, Youssef MA, Nehdi M. Utilizing shape memory alloys to enhance the performance and safety of civil infrastructure: a review. Can J Civ Eng 2007;34(9):1075–86.
[44] Cladera A, Oller E, Ribas C. Pilot experiences in the application of shape memory alloys in structural concrete. J Mater Civ Eng 2014;26(11).
[45] Raza S, et al. Shape memory alloy reinforcement for strengthening and self-centering of concrete structures-State of the art. Constr Build Mater 2022;324.

[46] Yaqub, M.A., C. Czaderski, S. Matthys. Externally applied iron based shape memory strips as shear reinforcement for concrete I-sections. in fib Symposium 2023, Building for the future: Durable, Sustainable, Resilient. 2023. Istanbul, Turkey.
[47] Yaqub, M.A., S. Matthys, C. Czaderski, Potential of memory steel reinforcement for shear strengthening of concrete bridge girders with I-sections, in IABSE Symposium Prague 2022: challenges for existing and oncoming structures. 2022, International Association for Bridge and Structural Engineering (IABSE): Prague, Czech Republic. p. 1180–1187.
[48] *S&P Resin 220 HP*: Technical data sheet, S&P Clever Reinforcement Company AG. 2022; Available from: ⟨https://www.sp-reinforcement.eu/en-EU/products/sp-resin-220-hp⟩.
[49] re-fer. re-plate 120/1.5 mm: Technical data sheet, re-fer Strengthening Solutions AG, Switzerland. 2023; Available from: ⟨https://www.re-fer.eu/en/re-plate/⟩.
[50] re-fer. re-bar 10 mm: Technical data sheet, re-fer Strengthening Solutions AG, Switzerland. 2023; Available from: ⟨https://www.re-fer.eu/en/re-bar/⟩.
[51] fib, Model Code for Concrete Structures 2010. 2013, International Federation for Structural Concrete: Lausanne, Switzerland. p. 402.
[52] Pan ZF, Li B, Lu ZT. Effective shear stiffness of diagonally cracked reinforced concrete beams. Eng Struct 2014;59:95–103.
[53] Collins MP, Mitchell D. Shear and torsion design of prestressed and non-prestressed concrete beams. J Prestress Concr Inst 1980;25(5):32–100.